INTERNATIONAL JOURNAL OF CLIMATOLOGY
Int. J. Climatol. (2014)
Published online in Wiley Online Library
(wileyonlinelibrary.com) DOI: 10.1002/joc.4226

RMetS
Royal Meteorological Society

Variability of the subtropical highs, African easterly jet and easterly wave intensities over North Africa and Arabian Peninsula in late summer

James Spinks[a] and Yuh-Lang Lin[a,b]*

[a] *Department of Energy and Environmental Systems: Atmospheric Science, North Carolina A&T State University, Greensboro, NC, USA*
[b] *Department of Physics & EES, North Carolina A&T State University, Greensboro, NC, USA*

ABSTRACT: The North African climate is analysed for August during a 32-year period using the European Centre for Medium Range Weather Forecast (ECMWF) global data set to investigate the intensity variability at 600 mb of the subtropical highs, Africa easterly jet (AEJ) with two embedded local wind maxima, and African easterly waves over North Africa and the Arabian Peninsula. The variability of these synoptic weather systems is higher in East Africa. The most noticeable variability of intensity occurred with easterly waves. Maintenance of easterly waves from the Arabian Peninsula into East Africa is dependent on strong zonal gradients from the AEJ through shear vorticity. These zonal gradients were induced by the strengthening of the subtropical highs and the presence of a westerly jet in Central Africa and south of the Arabian Peninsula. During positive ENSO periods, these systems are generally weaker while in negative periods are stronger. The focus of this research is to investigate the role of the Arabian High and eastern local wind maximum (LWM_E) on complementing the Saharan High and western local wind maximum (LWM_W). It is found that an intense local wind maximum in East Africa helps maintain the easterly waves and their westward propagation from the Arabian Peninsula.

KEY WORDS African easterly jet; Arabian Peninsula; easterly wave; North Africa; subtropical high; variability

Received 3 March 2014; Revised 2 November 2014; Accepted 4 November 2014

1. Introduction

Over North Africa and Arabian Peninsula, there exist several synoptic systems that influence weather patterns in late summer significantly, such as Saharan and Arabian Highs, the African easterly jet (AEJ) with two embedded local wind maximums (LWMs), and easterly waves over Arabia, African easterly waves (AEWs) in mid-troposphere, such as 600 mb. In particular, during the month of August, North Africa has been observed to be very active with easterly waves along with an unstable mid-tropospheric jet. In addition, North Africa experiences its most active month for precipitation in August.

Spinks *et al.* (2014) investigated the AEJ and local wind maxima in the west (LWM_W) and east (LWM_E) Africa, respectively, to the Saharan and Arabian Highs. In their study, an analysis of the European Centre for Medium-Range Weather Forecasts Intermediate Reanalysis (ERA-Interim or ERA-I) at 0.75 for the month of August over 32 years (1979–2010) was carried out to compare the differences of the AEJ's maintenance and formation associated with LWM_W and LWM_E. LWMs are embedded zonal wind maxima within the AEJ in West Africa around (17°N, 15°W) and East Africa around (15°N, 35°E) at 600 mb. The LWM_W is a permanent feature that lasts year around, but the LWM_E is a semi-permanent feature that is present when the Arabian high is intense, which is mainly during May, August, and October. The monthly mean for the LWM_W and LWM_E is 13.41 and 9.8 m s^{-1} with a variance of 0.9 and 1.9, respectively. It was found from the thermal wind relationship, the presence of the Saharan and Arabian Highs will increase easterly flow to the south of the anticyclonic centres because of the increased meridional geopotential gradient. This geopotential gradient along with the dominant influence from baroclinicity helps give the AEJ two distinct zonal maxima in East and West North Africa. The geostrophic wind maximum explains the locations of the LWM_E and LWM_W.

In this research, we plan to extend the study of Spinks *et al.* (2014) to investigate the yearly variability of AEJ, LWMs, easterly waves, and AEWs and their intensities over North Africa and the Arabian Peninsula during the same period of 1979–2010 for the month of August. The sensitivities of these features to El Niño Southern Oscillation (ENSO) will also be studied. Points of interest include displacements of the LWMs and anticyclonic systems, structure of the AEJ, and easterly wave intensities.

2. Background

The subtropical high-pressure systems over North Africa and the Red Sea have been investigated in previous studies

* Correspondence to: Y-L. Lin, 302H Gibbs Hall, EES/ISET, North Carolina A&T State University, 1601 E. Market Street, Greensboro, NC 27411, USA. E-mail: ylin@ncat.edu

to show their relationship with the AEJ. Chen (2005) described the formation and maintenance of the Saharan High through divergent fields of velocity potential. It was shown that the divergent centre was formed from east–west differential heating by thermal low heating (hot) and downward (cold) branch of the Indian Monsoon. Similar procedure was performed by Spinks et al. (2014) for the Arabian High. With the usage of a higher spatial resolution data set, two divergent centres were found respectively for the Saharan and Arabian Highs. In particular, the divergent centre over Arabia was more intense due to the higher temperatures and colder sinking air from the upper troposphere.

It is well known that the AEJ is formed through baroclinicity (Cook, 1999; Thorncroft and Blackburn, 1999; Comforth *et al.*, 2009; Wu *et al.*, 2009), but the existence of the LWMs within the AEJ are from the meridionally induced pressure gradient from the anticyclonic centres of the Saharan High and Arabian High. The Arabian High serves as a maintenance mechanism for the LWM_E, which, in turn, aids easterly waves propagating from a genesis area located between 45°E and 55°E along the southern coast of the Arabian Peninsula into East Africa (Lin *et al.*, 2013). Lin *et al.* also proposed that this genesis area of vorticity is induced by the convergence of cyclonic vorticity produced by northerly winds and southerly winds from the Highs over Arabian Peninsula and Indian Ocean.

The ENSO (Bjerknes, 1969; Philander, 1990) index will also be used in this research. In order to further understand the variability of the AEJ to African climate, it is necessary to investigate how ENSO affects climate changes in Africa. Hulme (2001) noted that ENSO is a possible key driver on potential African climate variability. Kruger and Shongwe (2004) examined whether ENSO had any effects on the inclination in temperature, in particular for the late austral summer period. They concluded that increases in late summer temperatures are not forced by the occurrence of ENSO and non-ENSO events (Collins, 2011). Semazzi and Indeje (1999) demonstrated how ENSO affects the rainfall variability in East Africa, in which they concluded that ENSO plays a significant role in determining the monthly seasonal rainfall patterns in the East African region. Collins (2011) investigated the temperature variability over Africa with comparisons to the ENSO index and concluded that in June, July, and August one can observe warming throughout the whole continent. Chen (2005) suggested the North African climate systems may well be established through the effects of ENSO on the Asian monsoon's east–west circulation and in turn on the Saharan High.

The rest of this article is organized as follows. In Section 2, we will describe the data to be used for this study. Based on the analyses of the data, the variability of subtropical highs, LWMs, and easterly waves will be analysed and discussed in Section 3. In Section 4, we will make an ENSO composite analysis to help understand the AEJ variability. Conclusions can be found in Section 5.

3. The Data

In this study, we will use the ECMWF-interim (ERA-I) reanalysis data with a spatial resolution of $0.75° \times 0.75°$ on a global grid for August between 1979 and 2010 (Dee *et al.*, 2011). It was demonstrated in Spinks *et al.* (2014) that the LWMs were reproduced in other data sets such as ECMWF 40-year reanalysis (ERA-40) at 2.5° (Uppala *et al.*, 2005), the National Centre of Environmental Prediction (NCEP) reanalysis at 2.5° (Kalnay *et al.*, 1996), and the Climate Forecasting System Reanalysis version 1 (CFSR) at 0.3° (Saha *et al.*, 2006). Over the years, climatological analyses of the AEJ were carried out using global model data with relatively low spatial resolutions. The NCEP, ERA-40, and ERA-I have been used the most to study the synoptic weather over North Africa. For consistency, the ERA-I will be used to further investigate the dynamics. With this data set, the variability and structure of the Saharan and Arabian Highs, LWMs, and vorticity fields can be analysed with climatological means.

The Multivariate ENSO Index (MEI) (Wolter, 1987; Wolter and Timlin, 1993, 1998, 2011) will be used to extract values and make composites of the synoptic situations over Africa for ENSO and non-ENSO seasons. Unlike other ENSO indices that use only SST, the MEI, as proposed by the National Oceanic and Atmospheric Administration (NOAA) Earth System Research Laboratory (ESRL), uses six major observed variables over the tropical Pacific. These six variables are: sea-level pressure (P), zonal (U) and meridional (V) components of the surface wind, sea-surface temperature (S), surface air temperature (A), and total cloudiness fraction of the sky (C). In addition, the MEI uses bimonthly values, so the indices for July–August and August–September were averaged to obtain the ENSO index for August.

4. Variability of subtropical highs, LWMs, and easterly waves

At mid-troposphere, such as 600 mb, the Saharan and Arabian Highs and their associated circulations can be shown by streamfunction (ψ) (Figure 1(a)). To the south of the highs, there exists an AEJ axis with two embedded LWMs in East and West Africa, respectively, which can be illustrated by the zonal wind field (Figure 1(b)). As the easterly waves propagate along the southern flank of the AEJ axis, the relative vorticity (ζ) field is used to show the intensity of easterly waves over North Africa (Figure 1(c)). As the streamfunction and zonal wind fields are used to identify the maxima for the Saharan and Arabian Highs and LWMs, the mean, variance, and displacement for these maxima can be seen in Tables 1 and 2. To obtain the averages for the subtropical highs and LWMs, a regional domain in West and East Africa was set up to calculate maximum values.

The Saharan High has a mean streamfunction value of $9.1\,m^2\,s^{-1}$ with a variance of 1.9 for the month of August (Table 1 and Figure 1(d)). Most of the streamfunction variance occurs just north of the subtropical highs and over the

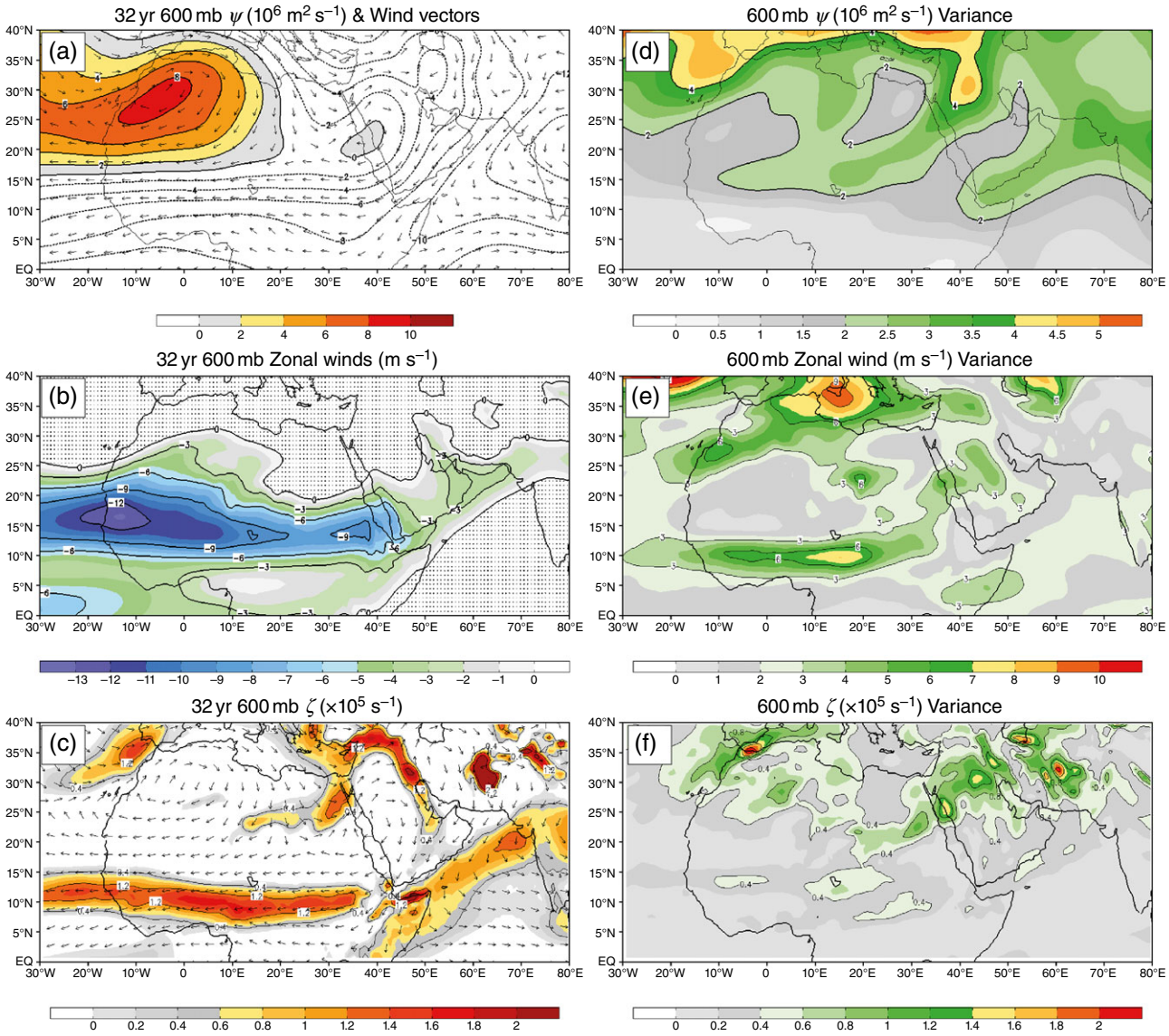

Figure 1. Averaged 32-year (1979–2010), 600 mb fields for August: (a) streamfunction ($\times 10^6$ m^2 s^{-1}) shaded with contours every 1×10^6 m^2 s^{-1} starting at 0 and wind vectors, (b) zonal wind (m s^{-1}) shaded with contours every 3 m s^{-1} and stippling representing positive zonal winds, (c) relative vorticity ($\times 10^{-5}$ s^{-1}) shaded and wind vectors, (d) streamfunction variance, (e) zonal wind variance, and (f) relative vorticity variance.

Table 1. August 1979–2010 average and variance of maximum streamfunction values associated with the Saharan and Arabian High in East and West Africa.

	Saharan high	Arabian high
Streamfunction average (m^2 s^{-1})	9.1	0.7
Streamfunction variance	1.9	2.2
Longitudinal average	4.7° W	38.1° E
Longitudinal variance	8.8	4.2
Latitudinal average	28.4° N	21.9° N
Latitudinal variance	2.8	4.4

Table 2. August 32-year (1979–2010) average and variance of maximum zonal winds associated with the LWM_W and LWM_E.

	LMW_W	LMW_E
Zonal average (m s^{-1})	−13.5	−9.9
Zonal variance	0.9	1.9
Longitudinal average	12.3 W	35.7 E
Longitudinal variance	23.8	9.4
Latitudinal average	16.2 N	13.8 N
Latitudinal variance	1.3	0.8

Mediterranean Sea that is associated with a mid-level subtropical jet stream. In the lower latitudes, the highest variance can be seen around the edges of the subtropical highs across North Africa and the Arabian Peninsula. On average, the Saharan High is located at (28.4°N, 4.7°W). The longitudinal and latitudinal variances are 8.8° and 2.8°, respectively. The LWM_W, which is located to the south of the Saharan High, has a zonal wind speed maximum of −13.5 ms^{-1} with a variance of 0.9. The highest variability of the AEJ exists over central North Africa, which is located around (10°N, 15°E) (Table 2 and Figure 1(e)).

On average, the LWM_W maximum is located at (16.2°N, 12.3°W). The longitudinal variance of the LWM_W is rather large because of displacement being between 20°W and 0°. Those anomalous years when the LWM_W is around 0° include 1986, 2000, 2002, and 2003. Exclusion of those years, the longitudinal variance of the LWM_W would decrease to 4.9°. The latitude of the LWM_W can reach as high as 18°N and as low as 13.5°N during August.

The Arabian High has a mean streamfunction value of $0.7\,m^2\,s^{-1}$ with a variance of 2.2 (Figure 1(d)) and averaged location at (21.9°N, 38.1°E). The longitudinal and latitudinal variances are 4.2° and 4.4°, respectively. The LWM_E, which is to the south of the Arabian High, has a mean of $-9.9\,m\,s^{-1}$ and a variance of 1.9 (Table 2 and Figure 1(e)). Compared to the LWM_W, the LWM_E does not vary as much in the longitudinal (35.7°E, 9.4°) and latitudinal (13.8°N, 0.8°) directions. The Arabian High and LWM_E are much smaller in size and weaker in intensity. The Arabian High and LWM_E are semi-permanent features in which Spinks *et al.* (2014) investigated the evolution of these systems for the entire year of 2006. Unlike the Saharan High and LWM_W, the Arabian High and LWM_E are formed in March and are matured by May. From June to late July, the systems weaken substantially while the Saharan High dominates most of North Africa, especially in West Africa. In August, the Arabian High and LWM_E can be seen in a developing or mature stage where the LWM_E is intense in East Africa.

The significance of the existence of LWM_E would aid the propagation and maintenance of easterly waves coming from the Arabian Peninsula into East Africa. Lin *et al.* (2013) explored the genesis of the pre-tropical Storm Debby AEW over the Arabian Peninsula. This wave is propagated along the easterly wind at 600 mb and was enhanced by orographic forcing associated with the Ethiopian Highlands and the LWM_E. Figure 1(c) depicts the relative vorticity field over Africa and the Arabian Peninsula. This relative vorticity region is an indicator of vorticity perturbation propagation paths south of the AEJ along the easterly wind flow. The most intense region of vorticity can be seen over central Africa between 0°E and 10°E. The vorticity field remains intense in East Africa and decreases slightly in the Arabian Peninsula. There exists a vorticity maximum at 10°N between 40°E and 50°E, which is a significant feature for genesis of vorticity perturbations that could lead to wave initiation once is advected into East Africa and enhanced by the Ethiopian Highlands and Darfur Mountains (Lin *et al.*, 2013). Other features from the vorticity field include the trough located between the Saharan and Arabian Highs and vorticity field on the east quadrant of the Arabian High. Analysing the variance in Figure 1(f) depicts the greatest variance of easterly wave intensities are at 5°W and 10°E to 35°E.

In order to understand how the AEJ makes contribution to the AEW, the mean relative vorticity field is decomposed into two components, namely the shear vorticity and curvature vorticity, which correspond to the first and second term of $\zeta = -\partial V/\partial n + V/R$, respectively. The shear vorticity ($-\partial V/\partial n > 0$) is the rate of change of wind speed normal to the direction of flow. In this instance, vorticity is primarily associated with the strength and gradient of the AEJ (Figure 2(a)). The curvature vorticity ($V/R_s > 0$) is the turning of the wind along a streamline (Figure 2(b)). This will express the AEW or easterly wave strength more properly instead of using the mean relative vorticity field. In Figure 2, the 32-year mean for shear and curvature vorticity is plotted for the month of August. Across North Africa between 10°N and 15°N, the shear vorticity is dominative and is caused by the strength of the AEJ's gradient. The shear vorticity extends from West Africa to the south of the Arabian Peninsula where it weakens along with the AEJ. Shear vorticity maximums can be seen at (12°N, 15°W), (10°N, 5°E), (12°N, 35°E), and (12°N, 45°E) across North Africa. The curvature vorticity is calculated by retaining the positive vorticity only, which gives a good signal to where the AEW troughs are located. In particular, curvature vorticity maxima are located at (10°–15°N, 30°–15°W), (8°–13°N, 0°–20°E), and (10°–15°N, 30°–40°E) across North Africa. The strongest indication of curvature vorticity is located on the lee of the Ethiopian Highlands. This would be due to the orographic effects from the Ethiopian Highlands producing vorticity perturbations during the diurnal cycles. The curvature vorticity maximum over the Ethiopian Highlands weakens over Sudan, but the shear vorticity maximum remains strong. The maintenance of shear vorticity comes from the presence of the LWM_E where the zonal wind gradient is strong along the AEJ in East Africa, particularly over Sudan. Once on the lee side of the Darfur Mountains at 20°E, the curvature vorticity maximum increases again and weakens at 0°. The curvature vorticity maximum increases in West Africa starting at 5°W and extends into the Atlantic Ocean. The shear and curvature vorticity both strengthens to the south of the Arabian Peninsula. This can be explained by the cyclonic convergence located (15°–20°N, 50°–60°E) from the easterlies of the Arabian High over the Arabian Peninsula and the westerlies from the Indian Ocean High (Lin *et al.*, 2013). This region is also the location of the Intertropical Convergence Zone (ITCZ).

The Saharan High, Arabian High, meridional geopotential, and temperature gradients play the biggest role in the intensity of the AEJ and its associated LWMs. The relative influences of dynamical processes on the intensities of the LWMs can be shown by analysing their correlations. Figure 3 shows the LWM_W zonal intensities versus the meridional geopotential gradient (Figure 3(a)), meridional temperature gradient (Figure 3(b)), and streamfunction (Figure 3(c)) between 1979 and 2010 for the month of August. The correlations between these variables are relatively high, which is to be expected because each variable contributes to the intensity of the LWM_W and overall AEJ. The streamfunction of Saharan High shows a correlation with the LWM_W of $r = 0.59$, the meridional geopotential gradient with $r = 0.80$, and the meridional temperature gradient with $r = 0.69$. As the LWM_W is mainly geostrophic, it is not surprising that the meridional geopotential gradient shows the highest correlation. The baroclinicity that

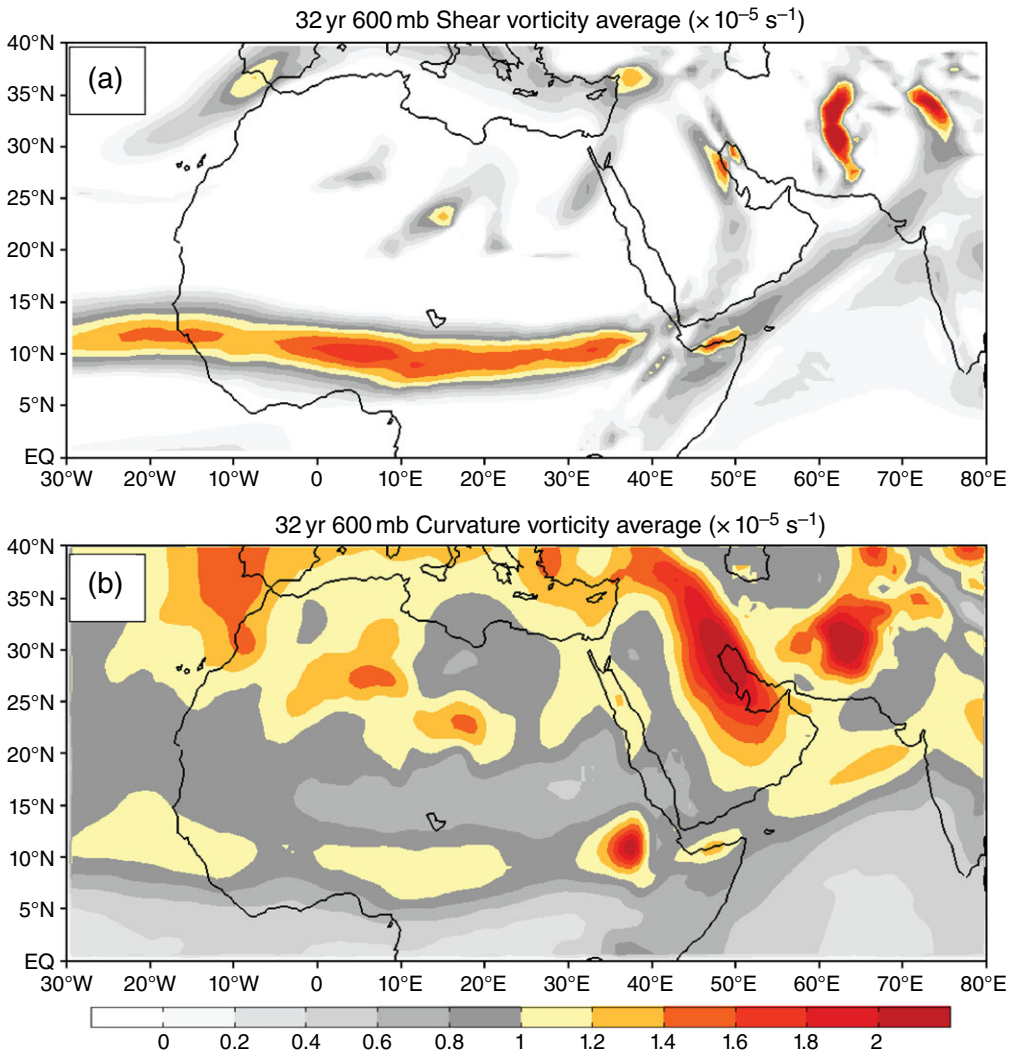

Figure 2. Averaged 32-year (1979–2010), 600 mb fields for August of (a) shear vorticity ($\times 10^{-5}$ s^{-1}) and (b) curvature vorticity ($\times 10^{-5}$ s^{-1}). The shaded contours are every 0.2 ($\times 10^{-5}$ s^{-1}) starting at 0.

plays the major role to the formation of the AEJ has a high correlation with AEJ intensity as well, but is not the major contributor to the intensity of the LWM_W. The baroclinicity explains the formation, while the maximum geopotential gradient that is located to the south of the Saharan high centre explains the increased easterly wind flow that results in the LWM_W (Spinks *et al.*, 2014). There are also noticeable years, where the LWM_W is very strong (LWM_W anomaly >1.0), such as 1984, 1994, 1998, 2000, 2007, and 2009.

The correlations for the LWM_E are much higher than the LWM_W (Figure (4)). The streamfunction shows a correlations of $r = 0.80$, the meridional geopotential gradient with $r = 0.95$, and the meridional temperature gradient with $r = 0.77$. Similar to the LWM_W, the meridional geopotential gradient has the highest correlation to the LWM_E intensity, while the baroclinicity contributes to intensity; it mainly explains more of the formation of the AEJ. Noticeable years where the LWM_E intensity is very strong ($LWM_E > 1.0$) include 1995, 1996, 1998, 1999, 2000, 2001, and 2010. Prior to 1995, the LWM_E is either neutral in intensity or very weak. Explanation of this could be due to ENSO. The Arabian High has its strongest year during this study in 1995 with a positive anomaly of 2.8, which is positively correlated with the LWM_E intensity. The two years that stand out most for the AEJ's varying intensity are the strong ENSO year in 1997 and the non-ENSO year of 1998 for August.

5. ENSO composite and analysis of subtropical highs, LWMs, and easterly waves

5.1. MEI index

As the variance has been established in the previous section, it is important to look into when the subtropical highs, LWMs, and easterly wave intensities are weak or strong. In other words, we are particularly interested in the effects of ENSO on the intensities of these synoptic systems. This can be accomplished by using the MEI (Figure 5). ENSO (non-ENSO) years are generally represented by the MEI index when it is greater (less) than

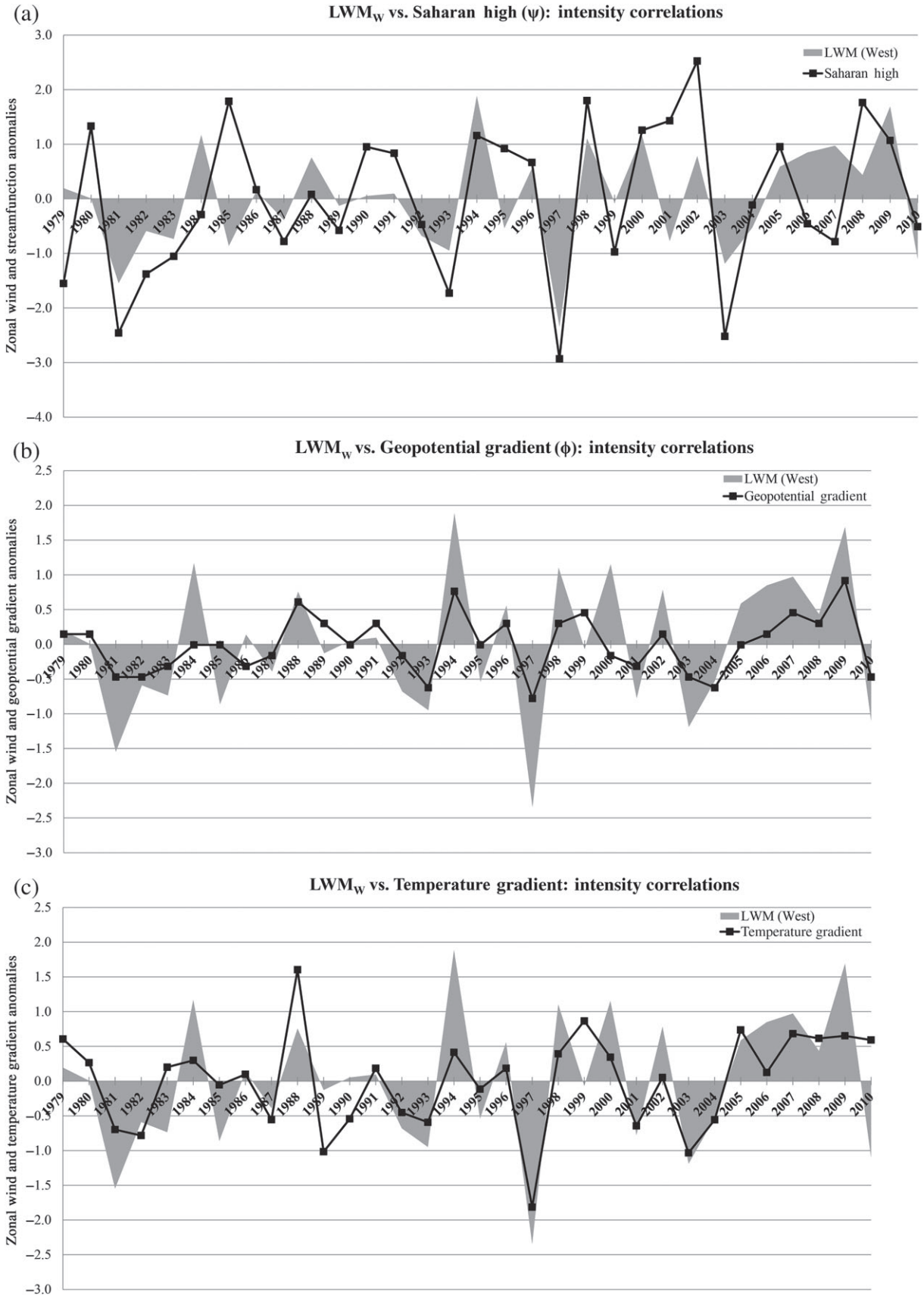

Figure 3. The 600 mb zonal wind maximum intensity (shaded) correlations to (a) meridional geopotential gradient, (b) meridional temperature gradient, and (c) streamfunction (Saharan High) intensity in West Africa for August during 1979–2010.

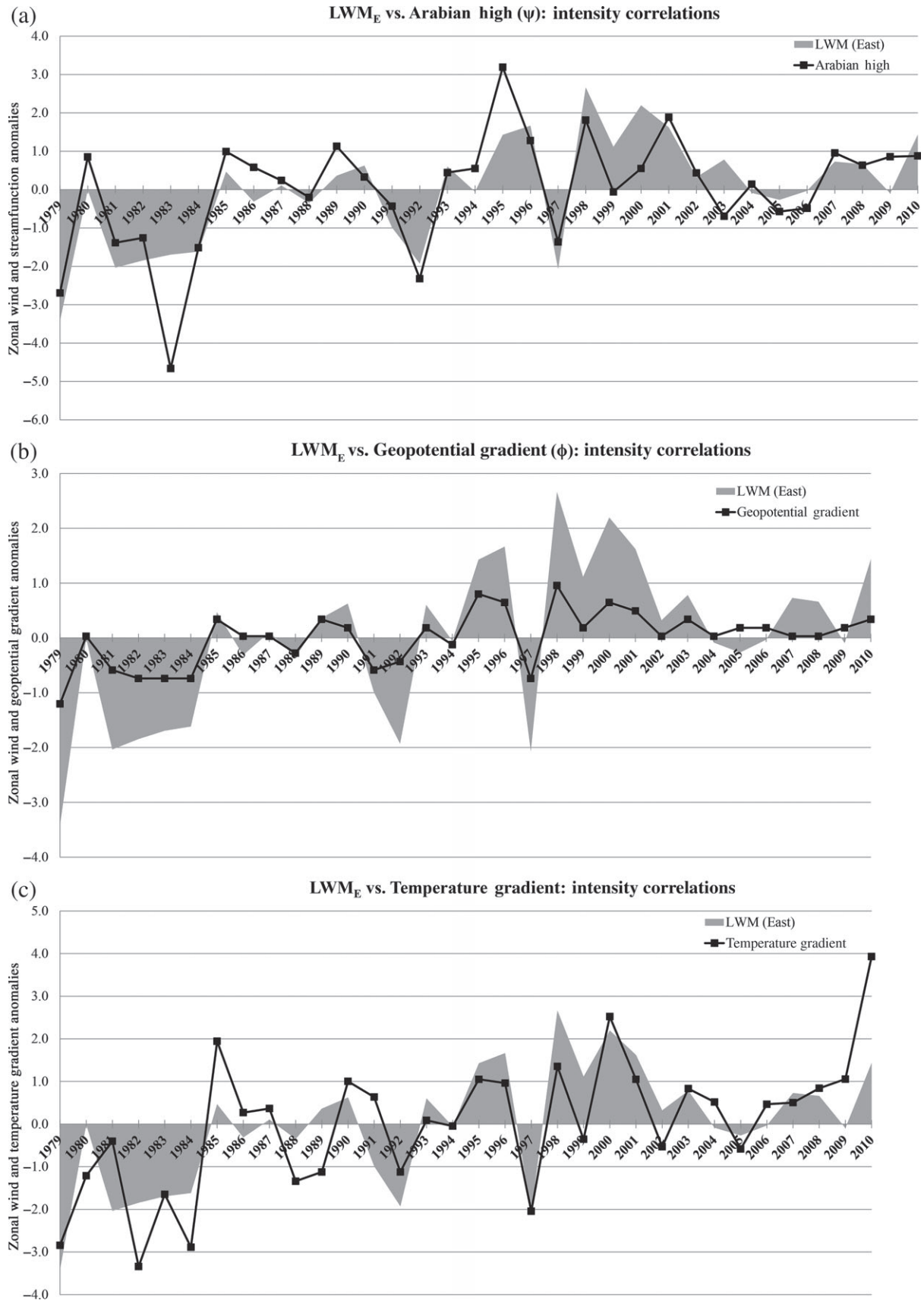

Figure 4. The 600 mb zonal wind maximum intensity (shaded) correlations to (a) meridional geopotential gradient, (b) meridional temperature gradient, and (c) streamfunction intensity in East Africa for August during 1979–2010.

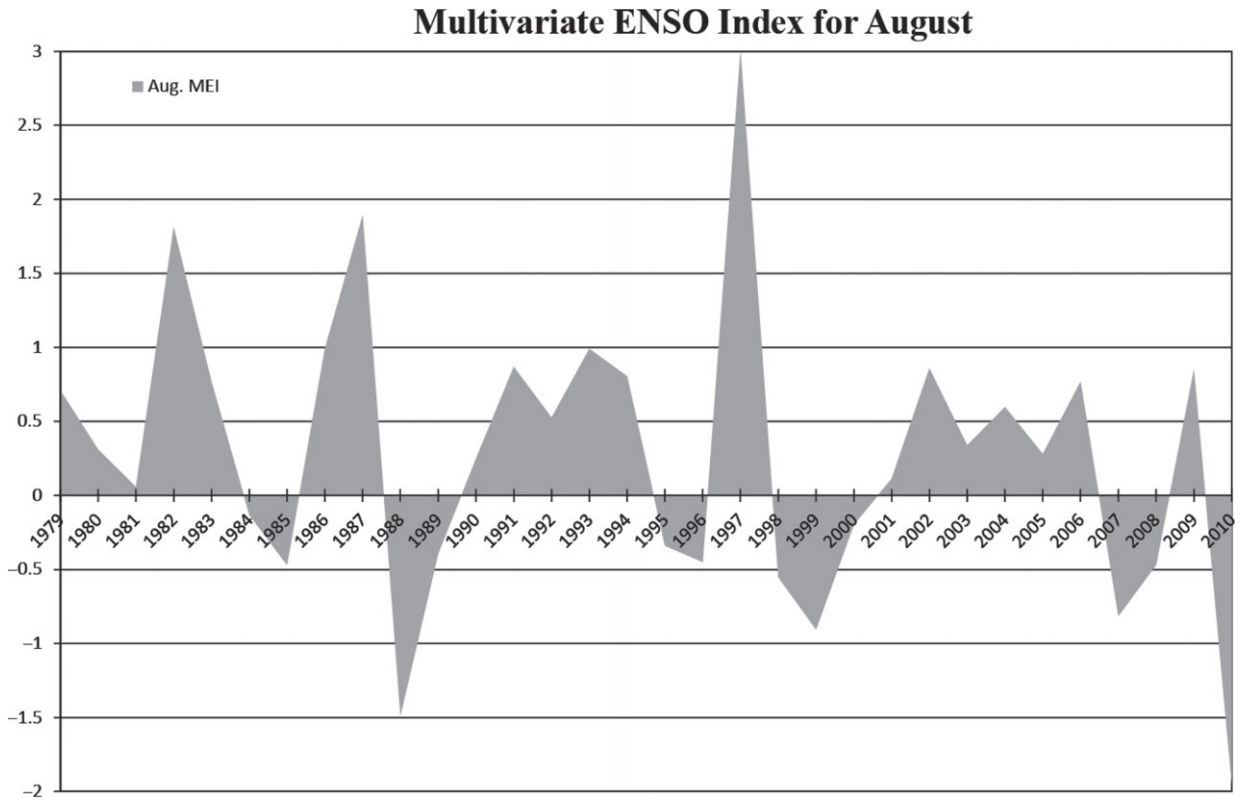

Figure 5. Multivariate ENSO Index for August during 1979–2010.

0.5 (−0.5). Notable ENSO years (MEI > 1) for August are 1982, 1986, 1987, 1993, and 1997, while notable non-ENSO years (MEI < −1) occurred in 1988 and 2010. Based on the 32 years of observed data from the MEI, the ENSO phase is generally positive for August.

5.2. ENSO composites

5.2.1. Subtropical highs composites

Figure 6 illustrates the ENSO variability of the Saharan and Arabian High using streamfunction. Results from this composite analysis reveal that these respected anticyclonic systems strengthen during Non-ENSO phases and weaken during positive ENSO phases. The Saharan High becomes broader during Non-ENSO phases while increasing in its intensity and circulation. The most noticeable change between phases comes from the Arabian High, which has a higher variance than the Saharan High at 2.2. The displacement of the anticyclonic systems is slightly higher in latitudes during non-ENSO phases, but not significant in change. The strengthening of the Arabian High means there is an increase in pressure, which will directly influence of the increase of intensity of the LWM_E. It is important to understand that the baroclinicity will also contribute to the intensity increase of the LWM_E, but the increase of pressure from the Arabian High will also increase the maximum geopotential gradient located to the south of the Arabian High. This in turn, will cause the LWM_E to have stronger easterly geostrophic winds causing a maximum that is near real zonal wind speeds (Spinks *et al.*, 2014). Figure 7 shows the difference of streamfunction between ENSO and non-ENSO (MEI > 0 to MEI < −0.5) phases. The most noticeable increase of intensity occurs to the south of subtropical high-pressure systems. South of the high systems is where the AEJ and LWMs are located. The positive values from the difference plot, which is between 5°N and 20°N across North Africa is representative of the streamfunction gradient. West Africa shows the biggest difference in intensity from the streamfunction difference versus East Africa. To the north of the subtropical highs, which is the Mediterranean jet, there is a decrease in streamfunction between ENSO and non-ENSO phases. In this instance, it appears that there is an inverted change of streamfunction intensity north of the subtropical highs versus south of the subtropical highs.

5.2.2. AEJ and LWMs composites

Figure 8 shows the ENSO composite of the AEJ. Similar to the highs, the AEJ's intensity increases (decreases) during negative (positive) ENSO years. The zonal wind speeds of the LWM_W does not change much in intensity between ENSO years, but the LWM_E's higher zonal variance shows an increase from 8 to 10 m s^{-1} during extreme ENSO to non-ENSO years, respectively. The AEJ structure also changes between ENSO years. During extreme ENSO years, the AEJ is weaker than average (Figure 1(b)) and broader in latitude. The zonal wind contours show a weaker gradient between 10°N and 15°N. The LWM_E is present and weak compared to the averaged intensity. During extreme non-ENSO years, the intensity of both LWMs increases, as well as the overall intensity of the

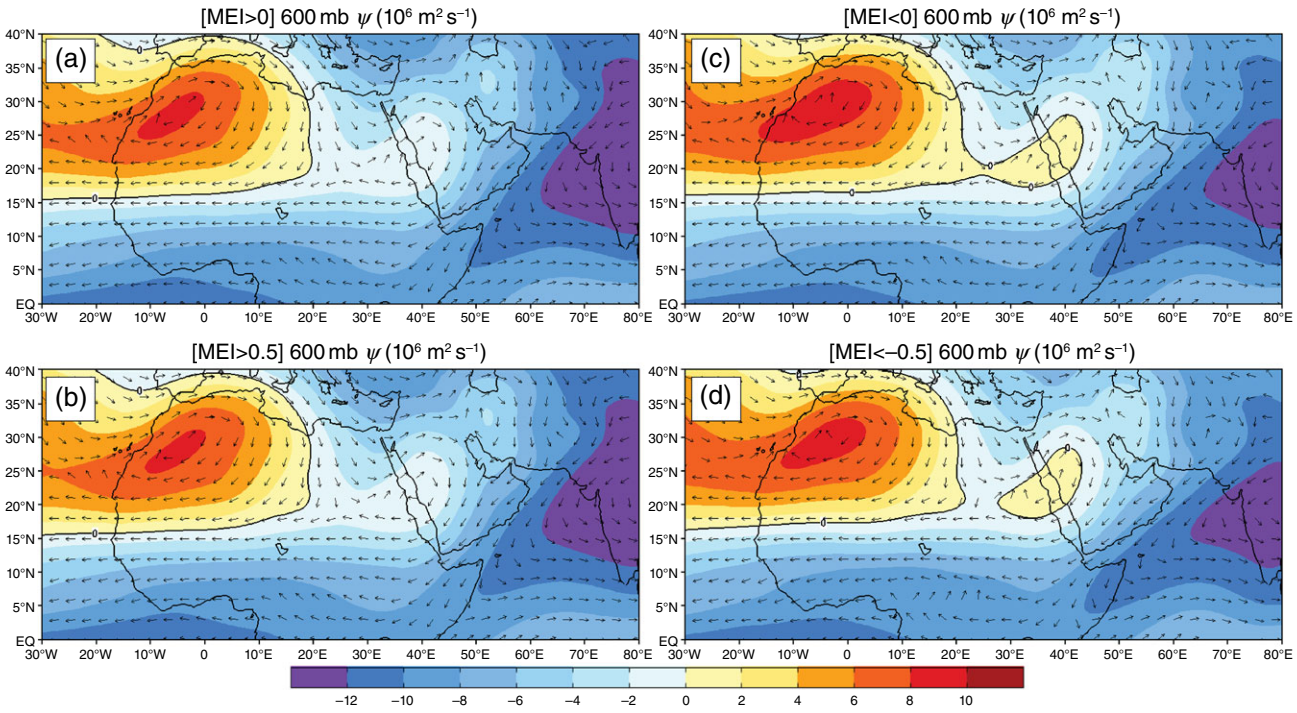

Figure 6. Composites of streamfunction at 600 mb using the MEI for ENSO: (a) MEI > 0 (all positive years), (b) MEI > 0.5 (ENSO years), (c) MEI < 0 (all negative years), and (d) MEI < −0.5 (non-ENSO years).

AEJ. The gradient of the zonal winds are strong between 10°N and 15°N, mainly due to the presence of the westerly jet into the mid-levels located at (5°–10°N, 10°–20°E). The LWM_W expands in size, but there is no significant change in intensity.

In Figure 9, the difference of the AEJ intensity can be seen between extreme ENSO and non-ENSO years. The LWM_W is located at (16.2°N, 12.3°W) on average for the month of August between 1979 and 2010. From the analysis of the difference plot, there is not a huge increase in intensity for the LWM_W, but there is noticeable increase to the northern and southern flanks of the AEJ in West Africa. Most of the increase of intensity between extreme ENSO and non-ENSO years will occur in East Africa and into the Arabian Peninsula. The LWM_E is located at (13.8°N, 35.7°E) on average. The LWM_E is clearly located in an area of high-intensity change, which is consistent with the high variance that occurs in East Africa. The extended AEJ that stretches into the Arabian Peninsula has a noticeable increase in intensity during extreme ENSO and non-ENSO year. What is most interesting about the difference analysis is the area located at (15°N, 55°E). This is the same location that Lin *et al.* (2013) investigated to be a genesis region for easterly waves because of cyclonic

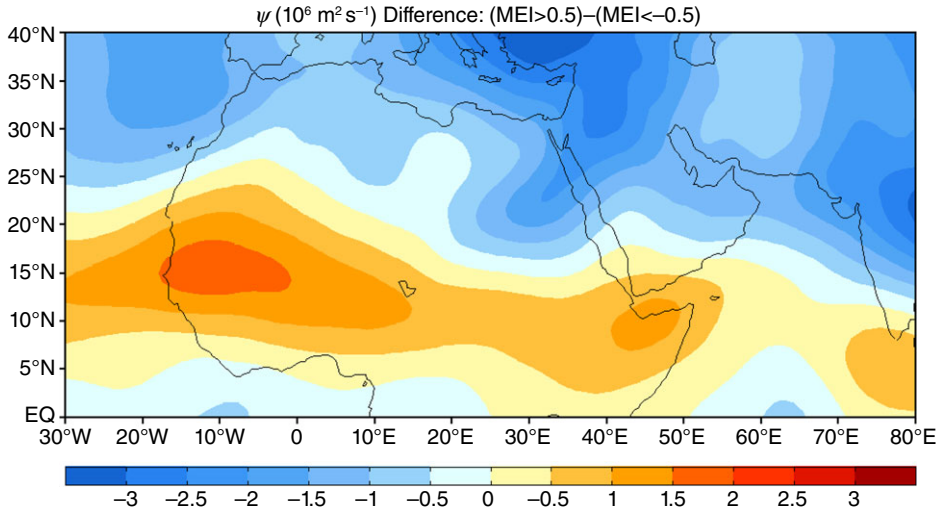

Figure 7. The 600 mb streamfunction ($\times 10^6$ m^2 s^{-1}) difference of extreme ENSO years (MEI > 0.5) and non-ENSO years (MEI < −0.5).

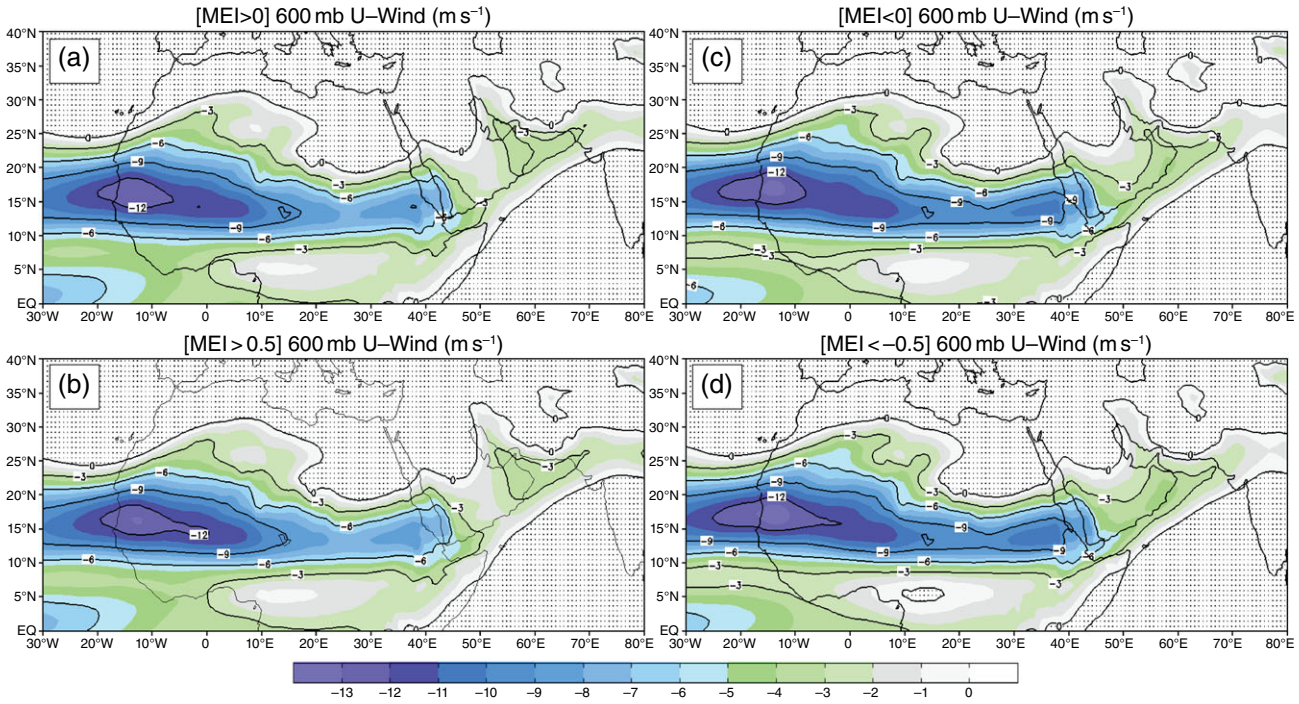

Figure 8. Composites of zonal wind (m s^{-1}) at 600 mb using the MEI for ENSO: (a) MEI > 0 (all positive years), (b) MEI > 0.5 (ENSO years), (c) MEI < 0 (all negative years), and (d) MEI < −0.5 (non-ENSO years). The stippling represents positive zonal winds.

convergence of the Arabian High and Indian Ocean High. Overall, the increase of easterly zonal wind intensity at 600 mb between 15°N and 20°N from extreme ENSO to non-ENSO years occurs over most of North Africa and southern Arabian Peninsula. The positive values located over the Mediterranean Sea and northern most part of the Arabian Peninsula is associated with the westerlies from the Mediterranean Jet.

5.2.3. *Shear and curvature vorticity composites*

The AEJ's 3 m s^{-1} zonal wind contour does not extend into the southern Arabian Peninsula during extreme ENSO seasons (Figure 8(b)), but does during extreme non-ENSO seasons (Figure 8(d)). The significance of the zonal wind increase over southern Arabia during extreme non-ENSO season means a strong positive zonal gradient ($\partial u/\partial y > 0$) will increase vorticity intensity ($\zeta = \partial v/\partial x - \partial u/\partial y$). As mention earlier, the mean relative vorticity was decomposed into shear vorticity ($-\partial V/\partial n > 0$) and curvature vorticity ($V/R_s > 0$) to isolate the effects from the AEJ zonal gradient and the AEWs, respectively.

The shear vorticity composite for ENSO years is illustrated in Figure 10. The shear vorticity field between 8°N and 15°N shows significance in intensity variability during extreme ENSO and non-ENSO years across West Africa, East Africa, and the Arabian Peninsula. It is noteworthy that the intensity of the shear vorticity field does not indicate an increase of the number of easterly waves, but explains the effect on vorticity intensity from the AEJ's zonal gradient. This composite analysis illustrates that shear vorticity intensity increase (decrease) during negative (positive) ENSO years. During extreme ENSO years, the shear vorticity field shows a decrease in intensity from the average (Figure 1(c)). The shear vorticity field over the Arabian Peninsula shows the most decrease in intensity compared to the average. Strong zonal winds of the AEJ, such as the 3 m s^{-1} contour, are not present over southern Arabia. Thus, shear vorticity intensity is inhibited slightly. The shear vorticity field in East Africa also shows a decrease in intensity, especially to the south of the region where the LWM_E is located.

In Figure 11, the extreme ENSO and non-ENSO difference plot illustrates clearly where the increased intensity of shear vorticity. Between 10°N to 16°N and 20°W to 40°E across North African is where the increased shear vorticity intensity occurs during extreme non-ENSO years. In particular, there are two distinct locations where there are shear vorticity maximums. One is located in West Africa centred at (15°N, 15°W) and the other is in East Africa centred at (12°N, 30°E). These maximums are located in the vicinity of the LWM_W and the LWM_E, which consistent with the shear vorticity increase (decrease) in intensity being associated with the increase (decrease) of the LWMs and overall AEJ intensity. There is another shear vorticity maximum located to the south of the Arabian Peninsula. This increased maximum is due to the increased easterly flow of the AEJ.

Vorticity that resulted from horizontal variations in the direction of the wind is called curvature vorticity. For positive curvature vorticity, the wind must be curving counterclockwise, or towards the left facing downward. The curvature vorticity composite in Figure 12 illustrates the easterly wave or AEW intensities across North Africa and the Arabian Peninsula. Unlike the shear vorticity, the

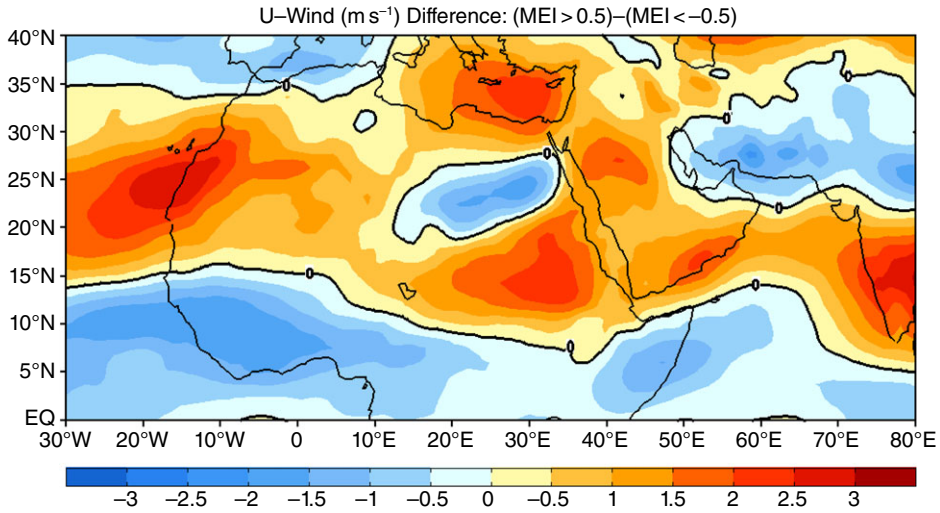

Figure 9. The 600 mb zonal wind (m s^{-1}) difference of extreme ENSO years (MEI > 0.5) and non-ENSO years (MEI < −0.5).

intensity of the curvature vorticity is weaker. Consistently between all ENSO seasons, there are four distinct areas across North Africa along the preferred region of AEW propagation where positive curvature vorticity is present. These areas are located at (10°–15°N, 30°–15°W), (8°–13°N, 0°–20°E), (10°–15°N, 30°–40°E) and (10°N, 45°E). Of these four areas, the curvature vorticity located over the Ethiopian Highlands in East Africa is the strongest. The curvature vorticity strength can be explained by vortex stretching and the conservation of Quasi-Geopotential Potential Vorticity (QGPV) over the high terrain in East Africa. When vorticity perturbations propagate over the Ethiopian Highlands, the atmospheric column is compressed and then stretched in which relative vorticity must change in order to conserve QGPV (Holton, 2004). This is most noticeable on the lee of the Ethiopian Highlands at (12°N, 38°E). During extreme ENSO years, the curvature vorticity is weaker than average across North Africa between 10°N and 15°N (Figure 12(b)).

During extreme non-ENSO years, the curvature vorticity over North Africa increases. Over the southern edge of the Arabian Peninsula which is along the ITCZ, the curvature vorticity is stronger (weaker) during ENSO (non-ENSO) years, but the shear vorticity weaker (stronger) during ENSO (non-ENSO) years. The variation of intensity of curvature vorticity is noticeable between ENSO and

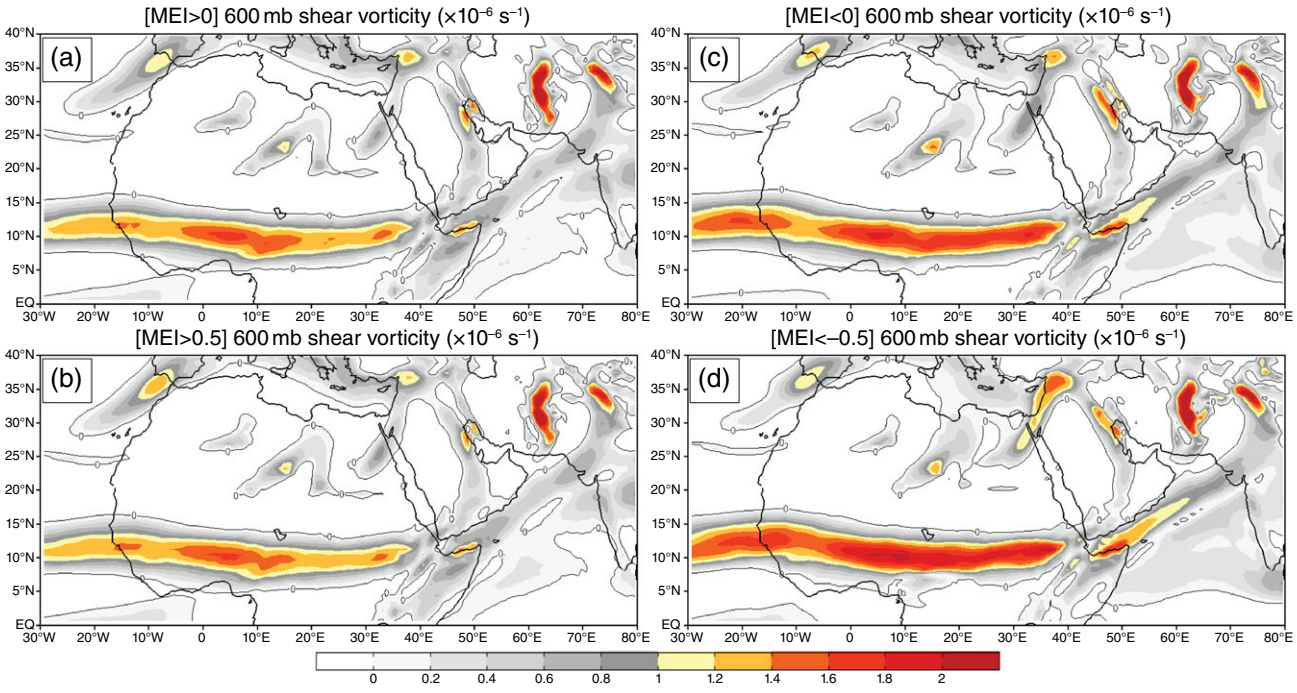

Figure 10. Composites of shear vorticity (×10^{-5} s^{-1}) at 600 mb using the MEI for ENSO: (a) MEI > 0 (all positive years), (b) MEI > 0.5 (ENSO years), (c) MEI < 0 (all negative years), and (d) MEI < −0.5 (non-ENSO years).

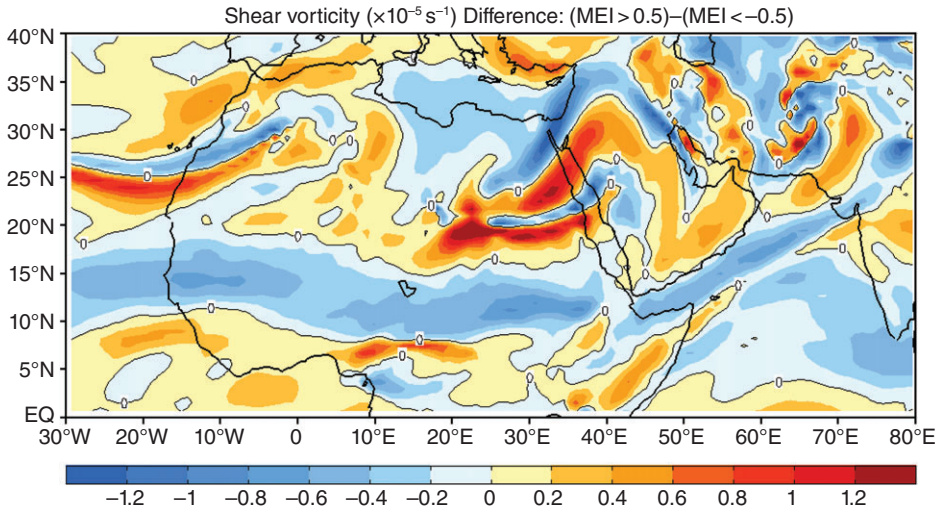

Figure 11. The 600 mb shear vorticity ($\times 10^{-5}$ s^{-1}) difference of extreme ENSO years (MEI > 0.5) and non-ENSO years (MEI < −0.5).

non-ENSO years and simultaneously increases and decreases in intensity with the anticyclones and AEJ. In Figure 13, the curvature vorticity difference plot has the highest variation of intensities (i.e. weak to strong) between extreme ENSO and non-ENSO at (10°N, 5 W–10°E) and (10°N, 15°–40°E). The variation is opposite over the southern Arabian Peninsula with the curvature vorticity weaker between ENSO and non-ENSO years. The highest variability of curvature vorticity occurs in East Africa and the Arabian Peninsula. Similar to the low variability of the Saharan High and LWM_W, the curvature vorticity maximum in West Africa does not show much variability of intensity.

5.3. East–west vertical circulation cell

So far in this research, it has been established that during extreme ENSO (non-ENSO) years the subtropical highs, AEJ with associated LWMs, and vorticity fields decrease (increase) in strength respectively. The shear vorticity field decrease (increase) is due to weaker (stronger) zonal gradient of the AEJ. The intensity of the LWM decrease (increase) with the weakening (strengthening) of the subtropical highs induced meridional geopotential gradient. The temperature is accounted for its relation to AEJ intensity, but structure and existence of the LWMs are due to the meridional geopotential gradient as the AEJ is mainly geostrophic. The meridional temperature gradient,

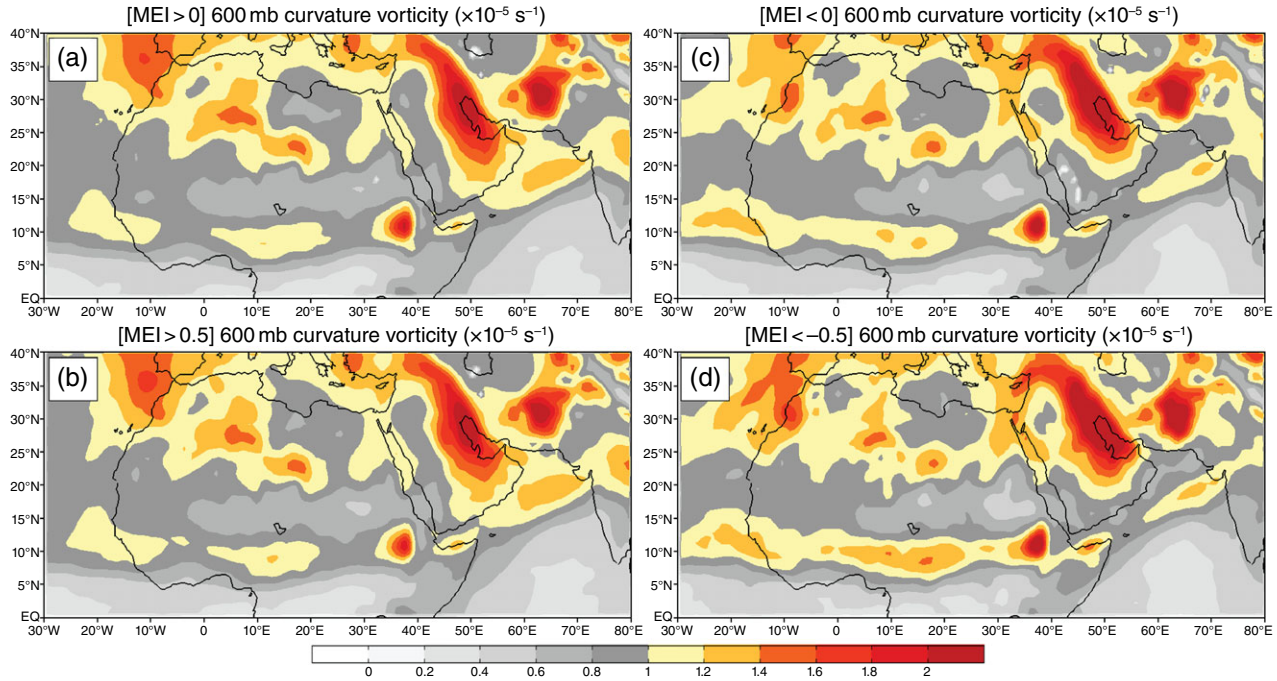

Figure 12. Composites of curvature vorticity ($\times 10^{-5}$ s^{-1}) at 600 mb using the MEI for ENSO: (a) MEI > 0 (all positive years), (b) MEI > 0.5 (ENSO years), (c) MEI < 0 (all negative years), and (d) MEI < −0.5 (non-ENSO years).

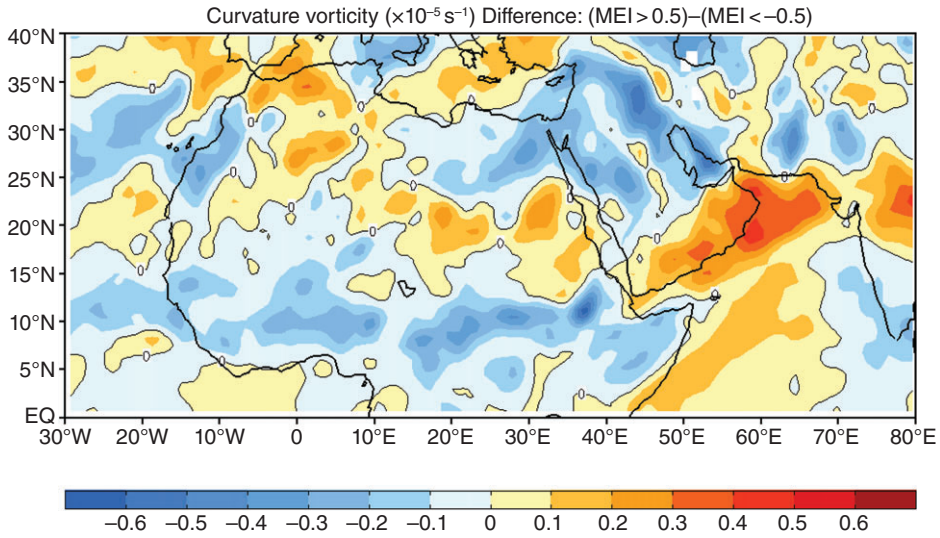

Figure 13. 600 mb curvature vorticity ($\times 10^{-5}$ s^{-1}) difference of extreme ENSO years (MEI > 0.5) and non-ENSO years (MEI < −0.5).

i.e. the baroclinicity, serves as the AEJ formation mechanism (Thorncroft and Blackburn, 1999; Wu *et al.*, 2009). Chen (2005) found that the LWM_W decreases (increases) with the Saharan High, while Spinks *et al.* (2014) found that the LWM_E decreases (increases) with the Arabian High. The next question is what causes the decrease and increase in the strength of the subtropical anticyclonic systems?

As mentioned in Section 1, Spinks *et al.* (2014) found that the Saharan and Arabian Highs are both maintained mainly by the east–west differential heating. Divergent centres over North Africa and the Arabian Peninsula are produced by the thermal heating which creates a low near surface and forces the air to rise and converge with the sinking cooler air from the upper atmosphere. Figure 14 illustrates the east–west circulation and vertical motion field over North Africa and the Arabian Peninsula along a vertical cross-section of 20°N. The latitude 20°N was chosen because the strongest vertical upward motions in the layer between 925 and 825 mb, based on figure 1 of Spinks *et al.* (2014). The strongest vertical motions are located over the mountain ranges across North Africa

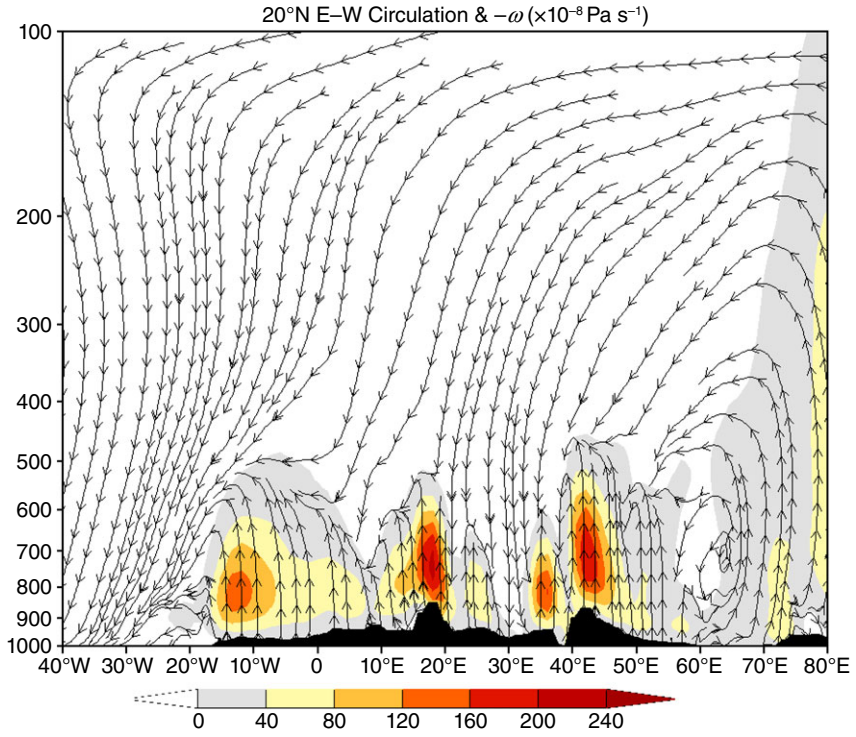

Figure 14. Averaged vertical cross section at 20°N of zonal wind and $-\omega$ ($\times 10^3$ Pa s^{-1}) for August during 32-year (1979–2010) period.

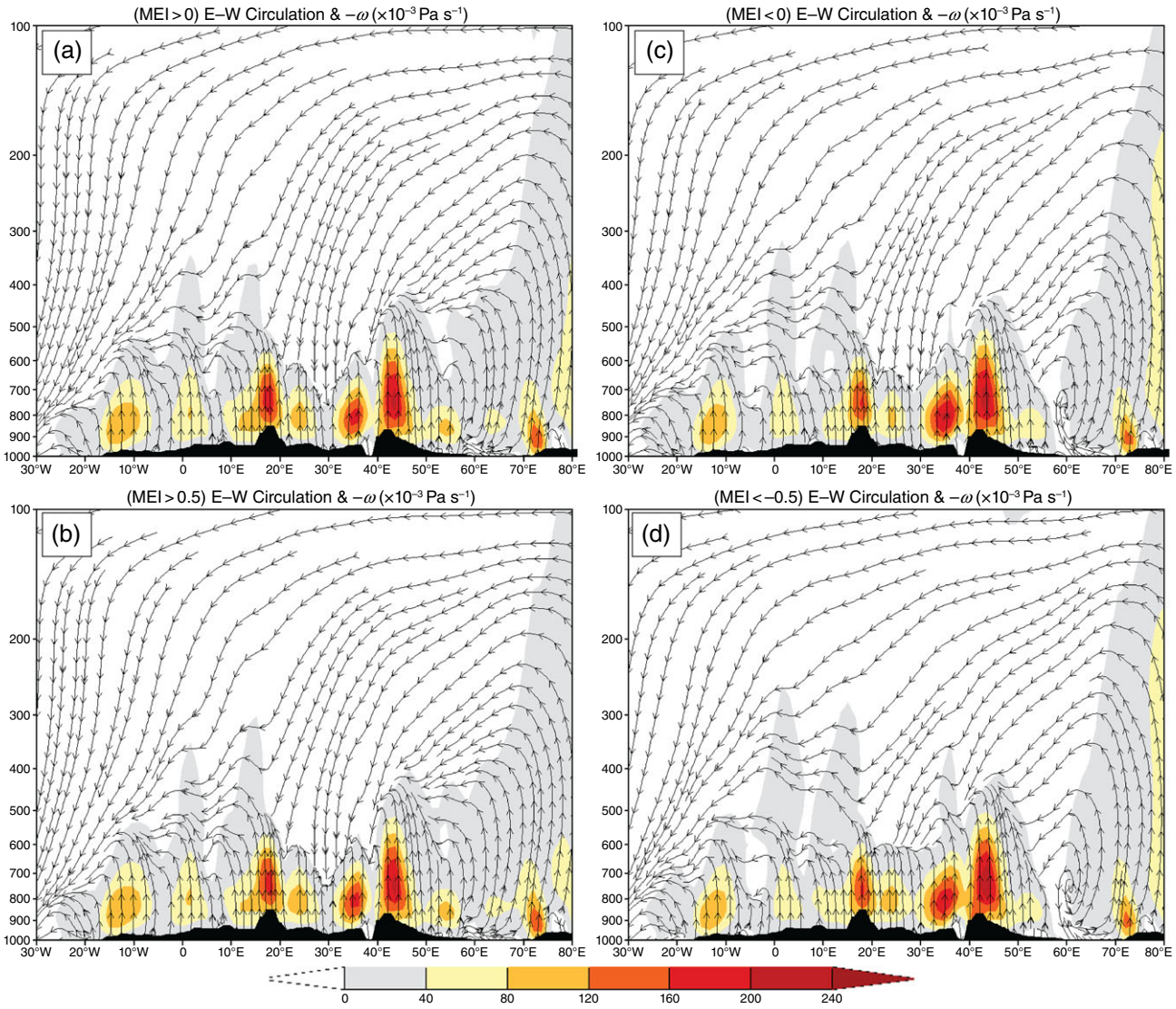

Figure 15. Composites of zonal wind and $-\omega$ ($\times 10^3$ Pa s^{-1}) using the MEI for ENSO: (a) MEI > 0 (all positive years), (b) MEI > 0.5 (ENSO years), (c) MEI < 0 (all negative years), and (d) MEI < −0.5 (non-ENSO years). Cross section is at 20°N.

and the Saharan and Arabian thermal lows. The divergence is seen in the mid-levels, such as in the layer of 700–500 mb. This was also illustrated from the velocity potential field at 600 mb in Chen (2005) and Spinks *et al.* (2014) which depicted the divergent centres associated with the strong convergence of the upward and downward motions. Between 60°E and 70°E, there exists a vertical circulation cell. The formation of this cell is attributed to the low-level westerlies associated with the Indian Ocean subtropical high, the intense upward motion associated with the Asian monsoon low, the upper-level tropical easterly jet, and the sinking cooler air from the northerlies over North Africa. The tropical easterly jet is in accelerating phase east of about 75°E where an upward branch of the east–west Walker cell is located and in decelerating phase west of it (Chen, 1982; Sathiyamoorthy *et al.*, 2006). This cell formation can be clearly illustrated from figure 1 of Spinks *et al.* (2014). Our question is: Does the presence of this cell and its associated east–west circulation patterns affect the intensity of the Saharan and Arabian Highs as both systems rely on the east–west differential heating?

It is noticeable from Figure 1(d)–(f) and Tables 1 and 2 that the highest variability of intensity from the subtropical highs, AEJ, and relative vorticity occurs in Ethiopia and South Sudan in East Africa and South Chad and Cameroon in Central Africa. West Africa does not experience the same variation of intensity. This is due to strong influence by thermal heating in West Africa. The variation of intensity over East Africa and the Arabian Peninsula can be explained by the presence and proximity of the east–west vertical circulation cell between 60°E and 70°E (Figure 15). Analysing the positive ENSO years, the east–west circulation cell is no longer present. This is due to the reduced zonal wind speeds from the tropical easterly jet in the upper atmosphere and the low-level westerlies associated with the high over the Indian Ocean. The divergence field associated with the convergence of vertical motions in the mid-atmosphere does not change

much. Between 25°E and 30°E, the drier air is produced by the downward motion through adiabatic warming, which acts as a wall between the Saharan and Arabian High.

During negative ENSO years, the east–west circulation cell is present. In contrast to the positive ENSO years during which the tropical easterly jet and low-level westerlies are weaker, the non-ENSO years induces stronger jets which will enhance the zonal components of the east–west circulation. The presence of this cell indicates that the divergence field is strong, which contributes to the intensity of the subtropical high-pressure systems, especially the Arabian High. With the enhancement of the Saharan and Arabian Highs, the pressure gradient increases the intensity of the LWM_W and LWM_E, respectively. The vertical motion over West and East Africa and Arabian Peninsula increases slightly, which is due to the enhancement of the thermal low heating during negative ENSO years.

6. Conclusions

At 600 mb during August (1979–2010), there exist the Saharan and Arabian Highs, AEJ with two embedded local wind maxima in West and East Africa, and easterly waves over Arabia and Africa easterly waves (AEWs) over Africa. The variability of these synoptic systems is examined. The highest variability occurs over Central Africa, Eastern Africa, and the Arabian Peninsula. For all synoptic systems present, positive (negative) ENSO years will decrease (increase) intensity. For West Africa, the Saharan High's intensity will either increase of decrease the intensity of the LWM_W. For East Africa, the Arabian High's intensity either increases or decreases the intensity of LWM_E. The LWM_E helps maintain the propagation of easterly waves, especially during extreme non-ENSO years where the westerly jet reaches into the mid-troposphere and enhances the AEJ zonal gradient. For the AEJ, the zonal gradient is weaker during ENSO years compared to that during non-ENSO years. The increased zonal gradient that increases shear vorticity is important for the variation of easterly wave intensity across North Africa and the Arabian Peninsula. When a strong zonal gradient is present over the Arabian Peninsula, it can help maintain easterly wave propagation. The curvature vorticity, which is weaker than the shear vorticity, has the highest variation in intensity between ENSO seasons at (10°N, 5°E–10°W) and (10°N, 15°–40°E) across North Africa. The variation is opposite over the southern Arabian Peninsula with the curvature vorticity weaker between ENSO and non-ENSO years. The curvature vorticity in West Africa has minimum change from extreme ENSO to non-ENSO years.

The higher variance in East Africa and the Arabian Peninsula is explained by the east–west vertical circulation cell located between 60°E and 70°E. The presence of this east–west circulation cell provides an indicator to the weakening (strengthening) of the Arabian High during positive (negative) ENSO years. During ENSO years, the east–west circulation cell was not present. During non-ENSO years, the east–west circulation was present. The weak variability of the Saharan High and LWM_W is due to its proximity from the east–west circulation cell. The Saharan and LWM_W are permanent features throughout the year and shifts in latitude during season changes. For August in particular, the Saharan and LWM_W will remain prominent features unless there is an anomalous shift to the east in longitude (around 0°) as observed in 2000, although intensity remained high for the synoptic systems.

East and West Africa's weather patterns are significantly different from each other. The common similarities are the correlations of intensity changes in synoptic systems with ENSO. The systems in East (West) Africa are smaller (larger) and weaker (stronger), but East Africa has a higher variability of intensity. Most importantly, this research connects the weather patterns in East and West Africa to each other, which is noteworthy for future studies of North African climate.

Acknowledgements

We would like to thank Dr. Solomon Bililign, the Director of NOAA ISET Centre, for his continuous encouragement in pursuing this study. Comments made by Dr. Jin Lee at NOAA ESRL, Dr. Bo-Wen Shen at the University of Maryland, Dr. Jing Zhang and Dr. Ademe Mekonnen at NC A&T State University are highly appreciated. We would also like to thank the reviewer for comments and suggestions. This research was supported by the National Oceanic and Atmospheric Administration Educational Partnership Program under Cooperative Agreement No: NA06OAR4810187 from 2006 to 2012 and by the National Science Foundation Awards AGS-1265783, HRD-1036563, OCI-1126543, and CNS-1429464.

References

Bjerknes J. 1969. Atmospheric teleconnections from the equatorial Pacific. *Mon. Weather Rev.* **97**: 163–172.

Chen T-C. 1982. On the kinetic energy budget of the summer mean flow at 200 mb in the tropics. *Tellus* **33**: 102–104.

Chen T-C. 2005. Maintenance of the midtropospheric North African summer circulation: Saharan high and African easterly jet. *J. Clim.* **18**: 2943–2962.

Collins JM. 2011. Temperature variability over Africa. *J. Clim.* **24**: 3649–3666, doi: 10.1175/2011JCLI3753.1.

Comforth RJ, Hoskins BJ, Thorncroft CD. 2009. Impact of moist processes on the African Easterly Jet–African Easterly Waves system. *Q. J. R. Meteorol. Soc.* **135**: 894–913.

Cook KH. 1999. Generation of the African easterly jet and its role in determining West African precipitation. *J. Clim.* **12**: 1165–1184.

Dee DP, Uppala SM, Simmons AJ, Berrisford P, Poli P, Kobayashi S, Andrae U, Balmaseda MA, Balsamo G, Bauer P, Bechtold P, Beljaars ACM, van de Berg L, Bidlot J, Bormann N, Delsol C, Dragani R, Fuentes M, Geer AJ, Haimberger L, Healy SB, Hersbach H, Hólm EV, Isaksen L, Kållberg P, Köhler M, Matricardi M, McNally AP, Monge-Sanz BM, Morcrette JJ, Park BK, Peubey C, de Rosnay P, Tavolato C, Thépaut JN, Vitart F. 2011. The ERA-Interim reanalysis: configuration and performance of the data assimilation system. *Q. J. R. Meteorol. Soc.* **137**: 553–597.

Holton JR. 2004. *An Introduction to Dynamic Meteorology*, 4th edn. Elsevier Academic Press: Burlington, MA.

Hulme M. 2001. Climate perspectives on Sahelian dessiccation: 1973–1998. *Global Environ. Change* **11**: 19–29.

Kalnay E, Kanamitsu M, Kistler R, Collins W, Deaven D, Gandin L, Iredell M, Saha S, White G, Woollen J, Zhu Y, Leetmaa A, Reynolds R, Chelliah M, Ebisuzaki W, Higgins W, Janowiak J, Mo KC, Ropelewski C, Wang J, Jenne R, Joseph D. 1996. The NCEP/NCAR 40-Year Reanalysis Project. *Bull. Am. Meteorol. Soc.* **77**: 437–471.

Kruger AC, Shongwe S. 2004. Temperature trends in South Africa: 1960–2003. *Int. J. Climatol.* **24**: 1929–1945.

Lin Y-L, Liu L, Tang G, Spinks J, Jones W. 2013. Origin of the pre-Tropical Strom Debby (2006) African easterly wave-mesoscale convective system. *Meteorol. Atmos. Phys.* **120**: 123–144.

Philander SGH. 1990. *El Niño, La Niña, and the Southern Oscillation*. Academic Press: London.

Saha S, Nadiga S, Thiaw C, Wang J, Wang W, Zhang Q, Van den Dool HM, Pan H-L, Moorthi S, Behringer D, Stokes D, Peña M, Lord S, White G, Ebisuzaki W, Peng P, Xie P. 2006. The NCEP Climate Forecast System. *J. Clim.* **19**: 3483–3517, doi: 10.1175/JCLI3812.1.

Sathiyamoorthy V, Pal PK, Joshi PC. 2006. Intraseasonal variability of the Tropical Easterly Jet. *Meteorol. Atmos. Phys.* **96**: 305–316.

Semazzi FHM, Indeje M. 1999. Inter-seasonal variability of ENSO rainfall signal over Africa. *J. African Meteorol. Soc.* **4**: 81–94.

Spinks J, Lin Y-L, Mekonnen A. 2014. Effects of the subtropical anticyclones over North Africa and Arabian Peninsula on the African easterly jet. *Int. J. Climatol.*, doi: 10.1002/joc.4017.

Thorncroft CD, Blackburn M. 1999. Maintenance of the African easterly jet. *Q. J. R. Meteorol. Soc.* **125**: 763–786.

Uppala SM, KÅllberg PW, Simmons AJ, Andrae U, Bechtold VDC, Fiorino M, Gibson JK, Haseler J, Hernandez A, Kelly GA, Li X, Onogi K, Saarinen S, Sokka N, Allan RP, Andersson E, Arpe K, Balmaseda MA, Beljaars ACM, Berg LVD, Bidlot J, Bormann N, Caires S, Chevallier F, Dethof A, Dragosavac M, Fisher M, Fuentes M, Hagemann S, Hólm E, Hoskins BJ, Isaksen L, Janssen PAEM, Jenne R, Mcnally AP, Mahfouf J-F, Morcrette J-J, Rayner NA, Saunders RW, Simon P, Sterl A, Trenberth KE, Untch A, Vasiljevic D, Viterbo P, Woollen J. 2005. The ERA-40 reanalysis. *Q. J. R. Meteorol. Soc.* **131**: 2961–3012, doi: 10.1256/qj.04.176.

Wolter K. 1987. The Southern Oscillation in surface circulation and climate over the tropical Atlantic, Eastern Pacific, and Indian Oceans as captured by cluster analysis. *J. Clim. Appl. Meteorol.* **26**: 540–558.

Wolter, K, Timlin MS. 1993. Monitoring ENSO in COADS with a seasonally adjusted principal component index. In *Proceedings of the 17th Climate Diagnostics Workshop*, Norman, OK, NOAA/NMC/CAC, NSSL, Oklahoma Clim. Survey, CIMMS and the School of Meteorol., Univ. Oklahoma, Norman, OK, 52–57.

Wolter K, Timlin MS. 1998. Measuring the strength of ENSO events – how does 1997/98 rank? *Weather* **53**: 315–324.

Wolter K, Timlin MS. 2011. El Niño/Southern Oscillation behaviour since 1871 as diagnosed in an extended multivariate ENSO index (MEI.ext). *Int. J. Climatol.* **31**: 1074–1087.

Wu M-LC, Reale O, Schubert SD, Suarez MJ, Koster RD, Pegion PJ. 2009. African easterly jet: Structure and maintenance. *J. Clim.* **22**: 4459–4480.

